ELSEVIER

Catalysis Today 52 (1999) 331–347

CATALYSIS TODAY

www.elsevier.com/locate/cattod

Kinetics and related engineering aspects of catalytic liquid-phase oxidation of *p*-xylene to terephthalic acid

Alberto Cincotti, Roberto Orrù, Giacomo Cao*

Dipartimento di Ingegneria Chimica e Materiali, Università degli Studi di Cagliari, Piazza d'Armi, 09123 Cagliari, Italy

Abstract

A lumped kinetic model for the liquid-phase oxidation of *p*-xylene to terephthalic acid catalyzed by cobalt naphtenate is presented. It is assumed that all the reactions are zeroth- and first-order with respect to gaseous and liquid reactants, respectively. The reliability of the developed model is investigated by comparison with experimental data obtained in an isothermal semi-batch oxidation reactor where the gas and the liquid phase are well mixed. The experiments included different values of the initial concentration of liquid reactants, two gaseous reactants (i.e. pure oxygen and air), various levels of catalyst concentration (from 1.67 to 33.3×10^{-4} mol/kg$_l$), and temperature values in the range 100–130°C. A semi-batch gas–liquid reactor model which accounts for the complex nature of the involved reaction network, as well as for inter- and intra-phase mass transport processes of both reactants and products is presented. The model, whose reliability is tested by comparison with suitable experimental data obtained in the semi-batch oxidation reactor, accounts also for the interaction between the involved chemical reactions and the precipitation kinetics of both 4-carboxybenzaldehyde and terephthalic acid. It is shown that the model describes the reactor behavior in any of the regimes which may prevail depending upon the operating conditions.

Keywords: Kinetics; Oxidation; *p*-Xylene; Terephthalic acid

1. Introduction

Direct oxidation by air or molecular oxygen of petroleum and natural gas derivatives is commonly employed in industry for the production of a wide variety of commercially important oxygenated compounds, i.e. the manufacture of benzaldehyde and benzoic acid from toluene, terephthalic acid from *p*-xylene and phenol from isopropylbenzene. Typically, transition metal complexes are employed as catalysts in order to reach high selectivities and convenient yields at mild operating conditions [1]. For the case of the production of terephthalic acid through liquid-phase oxidation of *p*-xylene, although this homolitic process has been the subject of a large number of patents and reports on the effect of several variables (i.e. catalyst and promoter concentration, nature of solvent, reaction temperature and so on) upon the oxidation rate [1,2], the available literature is not complete when looking for mechanism, kinetics or engineering aspects of this reaction, as recently pointed out by Raghavendrachar and Ramachandran [3].

For example, Emanuel and Gal [4] proposed a detailed radical-chain mechanism of the liquid-phase

*Corresponding author. Tel.: +39-70-675-5058; fax: +39-70-675-5067;
E-mail address: cao@visnu.dicm.unica.it (Giacomo Cao)

0920-5861/99/$ – see front matter
PII: S0920-5861(99)00086-3

cobalt catalyzed oxidation of *p*-xylene. However, the complexity of this reacting system clearly prevents the evaluation of the individual values of the kinetic constants by direct fitting of model results against experimental data, mostly because of the inability of measuring the concentration of the radical species. It is then apparent that suitable lumping procedures, leading to a reduction of the number of reactions and therefore of adjustable kinetic parameters, have to be developed. This procedure allows one to greatly simplify the design and simulation of reactor behavior since it significantly decreases the number of components whose diffusion–reaction phenomena have to be accounted for. Note that this approach has been previously adopted for the case of hydrocarbons autoxidation [5]. This aspect is of great interest because depending upon the experimental conditions adopted, the oxidation process can be either chemically rate- or mass-transfer limited [6]. In particular, at sufficiently high partial pressures of oxygen, the chemical rate is the controlling process, while mass transfer may become the controlling step of the overall process when using low oxygen partial pressures. Jacobi and Baerns [7] studied the effect of oxygen mass-transfer limitations on the overall oxidation rate and on the product distribution for the case of *p*-xylene oxidation catalyzed by cobalt-naphtenate. The interpretation of experimental data was performed using two different kinetic models depending on the controlling regime. In fact, in the case of chemically controlled regime the consumption rate of *p*-xylene was described by a second-power kinetic law with respect to *p*-xylene concentration, while a more complex relationship was proposed when oxygen mass-transfer limitation was the controlling step. Since a unique and realistic kinetic scheme was not provided, this interpretation appears to be clearly inadequate to simulate the reactor behavior in all possible operating regimes.

In the present work the liquid-phase oxidation of *p*-xylene to terephthalic acid catalyzed by cobalt naphtenate is described by an appropriate lumped kinetic scheme, where the reaction rate of each reactive step is assumed zeroth order reaction with respect to the transferring oxygen and first-order with respect to the liquid reactant. The former assumption is well established for alkylaromatics oxidation reactions as long as the oxygen partial pressure does not drop below a minimum value, i.e. 50–100 Torr [8]. By incorporating this kinetic model into an appropriate description of a semi-batch reactor, where the inter- and intra-phase mass transport of reactants and products are taken into account, the effect of mass transport limitations is investigated. The reliability of the developed model lumped kinetic scheme is tested by comparison with experimental data obtained in a semi-batch oxidation reactor. The effect of several operating variables (stirring speed, oxygen partial pressure, temperature, reactant concentration, catalyst concentration) is studied. In addition to chemical reaction and mass transport phenomena also precipitation plays an important role in liquid-phase *p*-xylene oxidation. In fact, the formation of two products, i.e. 4-carboxybenzaldehyde and terephthalic acid, occurs through a reaction precipitation process, since these compounds are formed by chemical reactions at concentration levels exceeding their solubility. In particular, 4-carboxybenzaldehyde is considered one of the most undesired contaminant of terephthalic acid, since its aldehyde group is unable to undergo condensation reaction with ethylene glycol during PET polymerization [9]. Only few investigations concerning reacting precipitation have been reported in literature [10,11] and references therein. This is particularly true when considering the simultaneous presence of gas–liquid mass transfer, chemical reaction and precipitation, which remain unexplored until recently [12,13]. In this work the interaction between chemical reaction and precipitation kinetics of both 4-carboxybenzaldehyde and terephthalic acid is analyzed theoretically. The latter phenomena are described by appropriate population balance equations incorporated in a semi-batch reactor model.

2. Experimental set-up and procedure

The experimental apparatus used in this work is described elsewhere [14]. Briefly, it consisted of a jacketed glass reactor maintained at the desired temperature through forced circulation of diathermic oil. Both the liquid and the gaseous phase were continuously stirred. The system was also equipped with a condenser in order to ensure complete condensation and recycle of the evaporated compounds. The reactor temperature was continuously monitored during the experimental runs with a thermometer. In a typical

experimental run, the reactor was charged with a proper amount of *p*-xylene and 200 cm^3 of methyl benzoate, as solvent. After the temperature reached the desired value, the catalyst, i.e. cobalt naphthenate, and 6 cm^3 of *p*-tolualdehyde, as promoter, were added. The gas (pure oxygen or air) was then continuously fed through the liquid. The experimental runs were carried out under the conditions summarized in Table 1, while maintaining fixed the initial *p*-tolualdehyde concentration (0.11 mol/kg_l). We caution the reader that working under 100% gaseous oxygen might be dangerous. The experimental runs reproducibility was verified by repeating each of them at least twice. The experimental runs reported in Table 1 were performed at 800 rpm since the influence of stirring speed on the product distribution was found to be negligible in the range 600–1000 rpm [14]. The reaction products were analyzed by high pressure liquid chromatography (HPLC). Analysis procedure details are reported elsewhere [15].

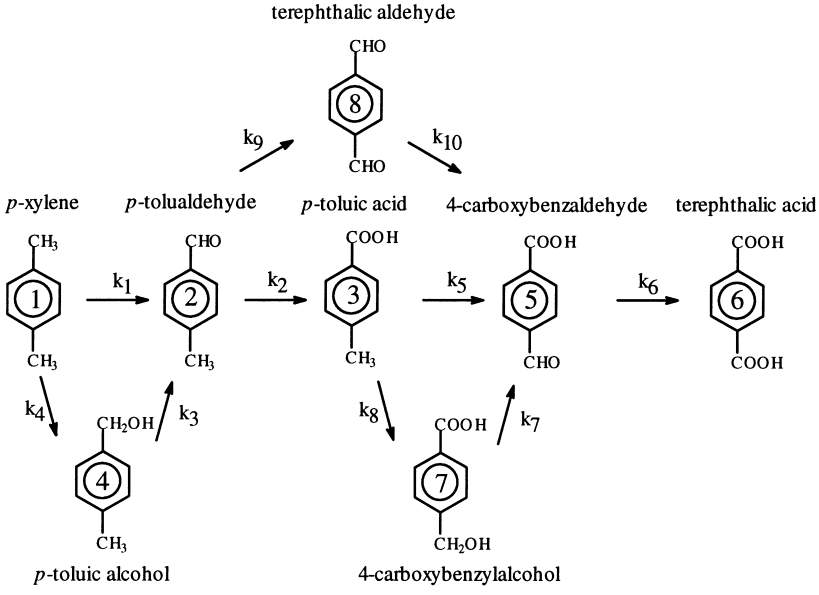

(1)

3. Lumped kinetic scheme and model equations

As emphasized in the introduction, the detailed kinetic mechanism proposed in the literature to describe the liquid-phase oxidation of *p*-xylene [4] needs to be simplified to be used in industrial reactor design and simulation. A proper simplified kinetic scheme may be obtained by reducing the complex mechanism into a small number of reactions, while retaining a description level detailed enough to characterize the final product distribution. By accounting for only the most important molecular species detected during the experimental runs, the following lumped kinetic scheme of *p*-xylene oxidation to terephthalic acid is proposed [16]:

where each reaction involves the addition of $\frac{1}{2}O_2$ and the corresponding kinetics are assumed zeroth and first-order with respect to oxygen and the liquid reactant, respectively.

The model of the semi-batch reactor previously described is developed under isothermal conditions and the description of the diffusion and reaction processes at the gas–liquid interface is simulated using the film theory. The mass balance for the *i*th component in the liquid film is given by:

$$D_i \frac{d^2 C_{i,f}}{ds^2} = -\sum_{j=1}^{N_R} V_{i,j} r_j, \quad i = 1,\ N_C \tag{2}$$

Table 1
Operating conditions for the experimental runs

Run	T (°C)	$C^0_{p\text{-xylene}}$ (mol/kg$_l$)	p_{g,O_2} (atm)	C_{cat} (mol/kg$_l$)$\times 10^4$
1	80	4.0	1.0	10.0
2	80	4.0	0.21	10.0
3	90	4.0	1.0	10.0
4	90	4.0	0.21	10.0
5	100	4.0	1.0	10.0
6	100	4.0	0.21	10.0
7	100	6.0	1.0	10.0
8	105	4.0	1.0	10.0
9	105	4.0	0.21	10.0
10	110	4.0	1.0	10.0
11	110	4.0	0.21	10.0
12	120	4.0	1.0	10.0
13	120	4.0	0.21	10.0
14	130	4.0	1.0	10.0
15	100	9.0	1.0	10.0
16	80	4.0	1.0	5.0
17	110	4.0	1.0	5.0
18	120	4.0	1.0	5.0
19	120	4.0	1.0	1.67
20	120	4.0	1.0	2.67
21	120	4.0	1.0	15.0
22	120	4.0	1.0	33.3

with boundary conditions for the dissolved oxygen:

$$-D_{O_2}\frac{dC_{O_2,f}}{ds} = k_{g,O_2}\left(p_{g,O_2} - H_{O_2}C^*_{O_2,f}\right) \quad \text{at } s = 0, \tag{3}$$

$$C_{O_2,f} = C_{O_2,1} \quad \text{at } s = \delta, \tag{4}$$

and for the volatile liquid reactants:

$$-D_i\frac{dC_{i,f}}{ds} = k_{g,i}\left(p_{g,i} - x^*_{i,f}p_{s,i}\right) \quad \text{at } s = 0; \quad i = 1,\ N_C, \tag{5}$$

where

$$x^*_{i,f} = \frac{C^*_{i,f}}{\sum_{m=1}^{N_C} C^*_{m,f}}, \quad i = 1,\ N_C, \tag{6}$$

$$C_{i,f} = C_{i,l} \quad \text{at } s = \delta; \quad i = l,\ N_C, \tag{7}$$

where the meaning of all symbols is reported in the notation. The system of PDEs (2)–(7) has been solved analytically only for a simpler kinetic scheme with respect to that shown in Eq. (1). The corresponding solution however is cumbersome and is reported elsewhere [14] for the sake of brevity. The numerical solution of general type proposed by Markos et al. [17] is more appropriate. The mass balances for the ith liquid reactant and for oxygen in the bulk liquid phase can be written as follows:

$$(\varepsilon_l - a_v\delta)\frac{dC_{i,l}}{dt} = a_vD_i\left[\left.\frac{dC_{i,f}}{ds}\right|_{s=0} - \left.\frac{dC_{i,f}}{ds}\right|_{s=\delta}\right] + (\varepsilon_l - a_v\delta)\sum_{j=1}^{N_R} v_{i,j}r_j \quad i = 1,\ N_C, \tag{8}$$

$$(\varepsilon_l - a_v\delta)\frac{dC_{O_2,l}}{dt} = -a_vD_{O_2}\left.\frac{dC_{O_2,f}}{ds}\right|_{s=\delta} - (\varepsilon_l - a_v\delta)\frac{1}{2}\sum_{j=1}^{N_R} r_j, \tag{9}$$

with the initial conditions:

$$C_{i,l} = C^0_{i,l}, \quad i = 1,\ N_C. \tag{10}$$

The first term of the right-hand side of Eq. (8) represents the mass flux of liquid reactant leaving the liquid film at the gas–liquid interface (s=0), which is condensed by the condenser and recycled back to the liquid bulk in the reactor. All the calculations were carried out by neglecting the partial pressure of the liquid reactants in the gas phase, i.e., $p_{g,i}$=0 in Eq. (5), and assuming the oxygen partial pressure equal to the inlet value. This assumption was checked a posteriori, by verifying, through an appropriate gas mass balance, that the oxygen depleted in the gaseous phase was only a small percentage (at most 5%) of the fed oxygen. The film model equations (2)–(7) and the overall liquid mass balances Eqs. (8)–(10) were solved simultaneously using standard numerical packages.

However when dealing with zeroth order reactions, care must be taken in setting all the reaction rates equal to zero if the oxygen concentration in the liquid film drops to zero. This situation occurs when the reaction is very fast compared to the diffusion rate of the gaseous reactant in the liquid film. In this case, the reaction goes to completion within the liquid film, while for slower reaction rates, it takes place both in the liquid film and in the liquid bulk. When the reaction rate is much slower than the rate of diffusion, most of the reaction occurs in the liquid bulk and the contribution of the reaction in the liquid film may be neglected. In order to describe in a continuous fashion

the transition between these regimes, which may occur during a single reaction batch due to the depletion of the liquid reactants, a unified approach for evaluating oxygen mass transfer has been introduced [14]. This is based on the comparison between the oxygen flux entering the liquid bulk and the maximum possible rate of oxygen consumption in the liquid bulk. Three situations may arise:

1. if the oxygen flux is larger than the maximum possible rate of oxygen consumption in the liquid bulk, the reactor is in the chemically controlled regime;
2. if the oxygen flux is smaller than the maximum possible rate of oxygen consumption in the liquid bulk, the oxidation process occurs both in the liquid film and in the liquid bulk;
3. if oxygen is completely depleted within the liquid film, no reaction occurs in the liquid bulk, i.e. the reaction takes place only in a portion of the liquid film.

It should be noted that the mass balances (Eqs. (8) and (9)) corresponding to situations (2) and (3) above need to be properly modified as shown in detail by Cao et al. [14] and Markos et al. [17]. It is also apparent that when the reactor is in the chemical controlled regime, the mass balances given by Eq. (8) may be written in terms of a simple homogeneous model as follows:

$$\frac{\mathrm{d}C_{i,l}}{\mathrm{d}t} = \sum_{j=1}^{N_\mathrm{R}} v_{i,j} r_j, \quad i = 1,\ N_\mathrm{C}, \tag{11}$$

along with the initial conditions (10), while neglecting the oxygen mass balance (9).

In order to simulate the precipitation phenomena of 4-carboxybenzaldehyde and terephthalic acid, the following assumptions are made:

- negligible agglomeration and disruption [13];
- precipitation due to supersaturation of 4-carboxybenzaldehyde and terephthalic acid;
- spherical crystals;
- growth rate independent from linear crystal dimension [10].

In particular by considering a homogeneous semi-batch reactor model, the mass balances for the non-precipitating species are identical to those reported in Eq. (11), while those for precipitating species are as follows:

$$\frac{\mathrm{d}C_{5,l}}{\mathrm{d}t} = k_5 C_{3,l} + k_7 C_{7,l} + k_{10} C_{8,l} - k_6 C_{5,l} - B'_5 - G'_5, \tag{12}$$

$$\frac{\mathrm{d}C_{6,l}}{\mathrm{d}t} = k_6 C_{5,l} - B'_6 - G'_6, \tag{13}$$

where B'_i and G'_i, i=5 and 6 are the mass based nucleation and growth rate, respectively. The population balances of the precipitated particles are:

$$\frac{\partial N_i}{\partial t} + G_i \frac{\partial N_i}{\partial L} = 0, \quad i = 5, 6, \tag{14}$$

where N_i is the population density of particles, G_i represents the linear growth rate, t the time and L is the coordinate of particle dimension. Eqs. (12) and (13) are coupled with Eqs. (10) and (11) together with the following initial and boundary conditions:

$$N_i = 0 \quad \text{at},\ t = 0 \ \ \forall L \quad i = 5, 6, \tag{15}$$

$$N_i = \frac{J_i}{G_i} \quad \text{at } L = L_{0,i},\ \forall t \quad i = 5, 6, \tag{16}$$

where J_i is the number nucleation rate and $L_{0,\,i}$ is the effective nucleic dimension. Note that the boundary condition (16) is used by several authors [18–20] and may become the dominant factor of crystal distribution. The mass based nucleation and growth rate equations are as follows:

$$B'_i = \frac{\pi}{6} \tilde{\rho}_{\mathrm{s},i} J_i L_{0,i}^3, \quad i = 5, 6, \tag{17}$$

$$G'_i = \int_{L_{0,i}}^{\infty} \pi G_i \tilde{\rho}_{\mathrm{s},\,i} L^2 N_i(L)\, \mathrm{d}L, \quad i = 5, 6, \tag{18}$$

where $\pi/6$ and π are related to the assumption of spherical crystals, $\tilde{\rho}_{\mathrm{s},i}$ is the crystal density, and the corresponding number rate of nucleation and linear crystal growth rate are expressed through the following equations [13]:

$$J_i = \bar{k}_{n,\,i} \left(C_{i,l} - C_{i,\,\mathrm{sat}}\right)^{n_i}, \quad i = 5,\ 6 \tag{19}$$

$$G_i = \bar{k}_{\mathrm{g},\,i} \left(C_{i,l} - C_{i,\,\mathrm{sat}}\right)^{g_i}, \quad i = 5,\ 6 \tag{20}$$

where $\bar{k}_{n,i}$ and $\bar{k}_{g,i}$ are the nucleation and growth rate constant, respectively, n_i and g_i are the orders of nucleation and growth, respectively, and $C_{i,\,\mathrm{sat}}$ is the

equilibrium saturation concentration. The governing balance equations are in the form of a system of ordinary and partial differential equations. A backward finite-difference scheme was adopted for the spatial derivative appearing in the population balances (14) in order to obtain a set of ordinary differential equations which were solved as an initial value problem using standard routines. During the computations, the value of the finite difference points was generally kept as 600 and the integral appearing in Eq. (19) was also solved numerically using standard routines [21].

4. Comparison with experimental data

4.1. Effect of temperature and oxygen partial pressure

When the experimental runs were carried out up to *p*-xylene conversion value of about 14%, the molecular species detected experimentally were only those indicated by the numbers 1–4 in the lumped kinetic scheme (1). Thus, in order to better understand the behavior of the reactor, it is convenient to first consider the overall oxygen uptake, U_{O_2} computed through the following relationship:

$$U_{O_2} = \tfrac{1}{2}\left(C_{2,l} - C^0_{2,l} + 2C_{3,l} + C_{4,l}\right), \tag{21}$$

where C_i represent the experimentally measured concentrations of the reaction products. A typical plot of the overall amount of oxygen consumed in the liquid phase as a function of time is shown in Fig. 1 for different temperature values. From the slope of these curves it is possible to obtain at each time value, the overall rate of oxygen uptake, R_{O_2}. In particular, the initial uptake rate values, $R^0_{O_2}$, are shown in Fig. 2 as a function of temperature. Note that two set of experimental data are reported, depending upon whether pure oxygen or air was fed to the reactor, but all involving the same initial composition of the liquid phase. From the Arrhenius-like plot of $R^0_{O_2}$ as a function of temperature shown in Fig. 2, some interesting conclusion about the reactor operating regimes can be drawn. At low temperature values, the reactor operates in the chemically controlled regime. The rate of oxygen uptake is the same whether pure oxygen or air is used, thus confirming that the chemical reaction is zeroth order with respect to oxygen. Moreover, the apparent activation energy is equal to about 15 kcal/mol, i.e., a value typical of oxidation reactions [22–24]. On the other hand, at higher temperature values

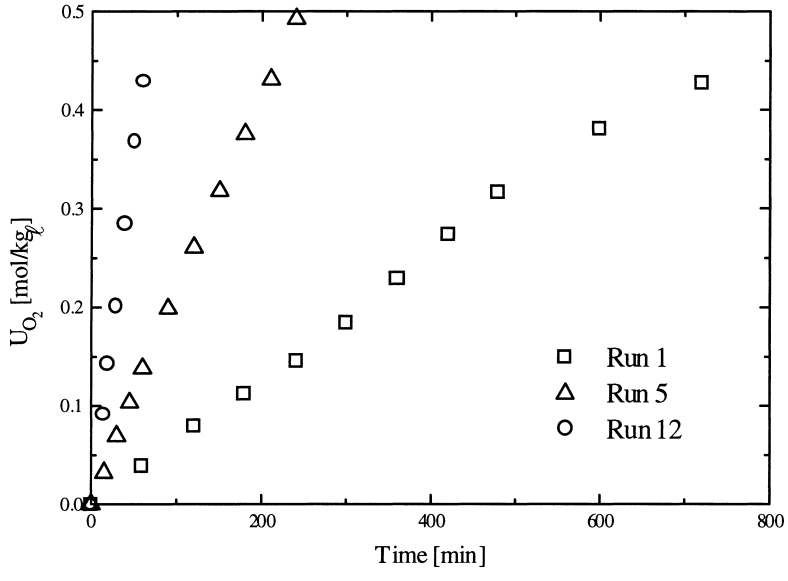

Fig. 1. Overall oxygen uptake, U_{O_2}, as a function of time for different temperature values.

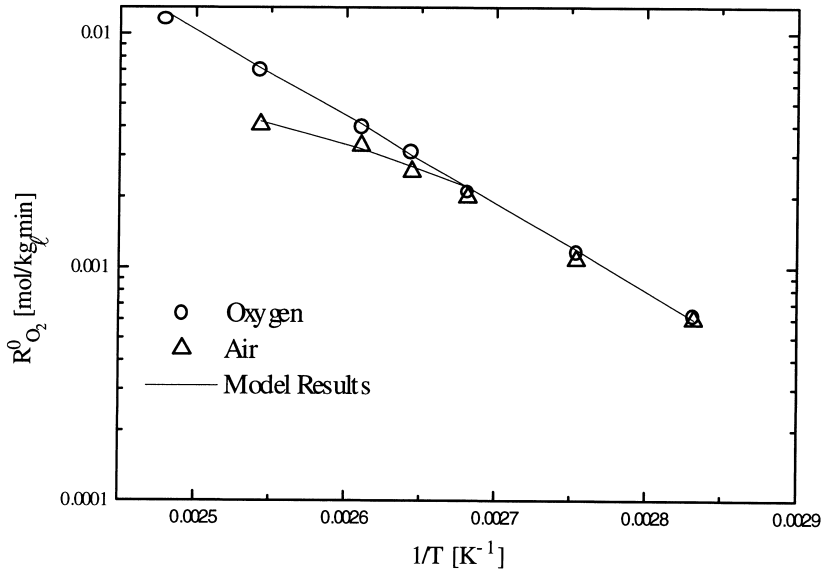

Fig. 2. Comparison between calculated and experimental values of the initial uptake rate of oxygen, $R^0_{O_2}$, as a function of temperature and oxygen partial pressure: runs 1–6 and 8–14 in Table 1.

diffusional limitations become important. These arise first in the experiments performed with air, as indicated by the deviation from linearity exhibited by the corresponding data in the Arrhenius plot in Fig. 2. A further support is given by the apparent activation energy value, which can be estimated from the two data at higher temperature for air oxidation as given by about 4 kcal/mol, a value typical of mass transfer limited processes. The experimental data relative to pure oxygen seem to lie on the same straight line on the Arrhenius plot in Fig. 2, thus indicating that, in this case the reactor operates in the chemically controlled regime in the entire temperature range.

Consequently, we evaluate the rate constants of the four reactions 1–4 of the lumped scheme (1) by considering only the experimental data obtained using oxygen in the feedstream, where diffusional resistances are not involved. For this situation, the model (2)–(10) then reduces to the homogeneous model (10) and (11). The values of the kinetic constants are then estimated by fitting the time evolution of the experimental product composition of runs 1, 3, 5, 8, 10 and 12 in Table 1 through a non-linear least-square procedure. A typical comparison between model results and experimental data is shown in Fig. 3, where it can be seen that the obtained agreement is in general satisfactory. Even though not shown here, also the experimental runs with air in the feed streams, which fall in the chemically controlled regime (i.e., runs 2, 4 and 6 in Table 1) are equally well reproduced by the model. Moreover, from the Arrhenius plot shown in Fig. 4(a), it can be seen that the absolute values of the rate constant k_1 lie on a straight line whose slope provides an apparent activation energy value of 14.6 kcal/mol, which is in good agreement with those reported in the literature for methyl-*p*-toluate oxidation [25] and for *o*-xylene oxidation [26]. Similar plots are obtained for the reactivity ratios $p_j=k_j/k_1, j=2–4$ as shown in Fig. 4(b). By maintaining fixed the value of the first four rate constants 1–4 calculated previously for low *p*-xylene conversion, the values of the remaining rate constants appearing in the lumped kinetic scheme (1) have been then estimated by fitting the time evolution of the experimental product composition of runs 10, 12 and 14. These are conducted up to higher values of *p*-xylene conversion, thus leading to a significant production of terephthalic acid. The comparison between model results and measured data is reported elsewhere [16], where it can be seen that the obtained agreement is in general satisfactory. This allows us to conclude that the proposed lumped kinetic scheme (1) retains a level of process description detailed enough to characterize the distribution of the most important products even when considering

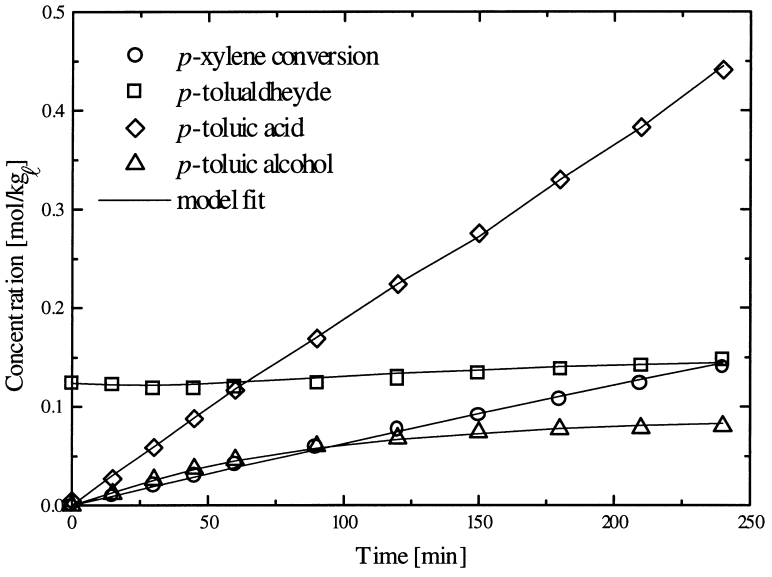

Fig. 3. Calculated versus experimental values of product concentration and *p*-xylene conversion as a function of time: run 5 in Table 1.

high *p*-xylene conversion. The numerical values of the Arrhenius parameters of the rate constant k_1 and of the nine reactivity ratios p_j are summarized in Table 2.

4.2. Effect of mass transfer phenomena

We can now turn to the evaluation of the liquid phase mass transfer coefficient, $k_l = D_{O_2}/\delta$. In particular, we consider the experimental run at 110°C with air in the feedstream (i.e., run 11 in Table 1) where, as it is clearly seen in Fig. 2, the shift from the kinetic to the diffusion controlled regime is estimated, the experimental data measured under these conditions are best suited to estimate the coefficient, k_l. In particular, we use the complete model (2)–(10), for which the value of physicochemical parameters are reported elsewhere [14], and estimate the parameter k_1 by fitting the measured values of the overall amount of oxygen consumed in the liquid phase as a function of time, obtained by operating the reactor both with pure oxygen and air at 110°C as shown in Fig. 5. It should be noted that the sought value of k_l is a rather specific one since it makes the model (2)–(10) able to predict the shift from the kinetic (oxygen run) to the mass transfer regime (air run) by only changing the oxygen partial pressure in the BC (3), while maintaining fixed the kinetic parameters, k_j, j=1–4 estimated above. A comparison between experimental data and model predictions at 110°C, for the best fitting value of the liquid mass transfer coefficient (k_l=2.8 cm/min) is shown in Fig. 5. This compares reasonably well with the values given by semiempirical literature relationships, such as k_l=4.86 cm/min obtained through the correlation of Calderbank and Moo-Young [27].

The value of k_l at temperature values other than 110°C, can be estimated from the k_l value obtained

Table 2
Numerical values for the Arrhenius parameters of the reactivity ratios for the reactions of the lumped kinetic scheme (1): $p_j=k_j/k_1$, where $k_1=A_1 \exp(-E_1/RT)$[a]

Reaction	p_j (110°C)[b]	$\Delta E_j=E_j-E_1$ (kcal/mol)
2	37.1	−4.748
3	24.6	59.542
4	0.70	2.069
5	0.32	0.0507
6	7.43	25.017
7	24.8	50.090
8	0.043	0.238
9	0.213	0.102
10	1.01	−0.694

[a] A_1=159 600 min^{-1}; E_1=14.600 kcal/mol.
[b] $p_j(T)=p_j(110°C) \exp(-(E_j(1/T-1/383)/R)$.

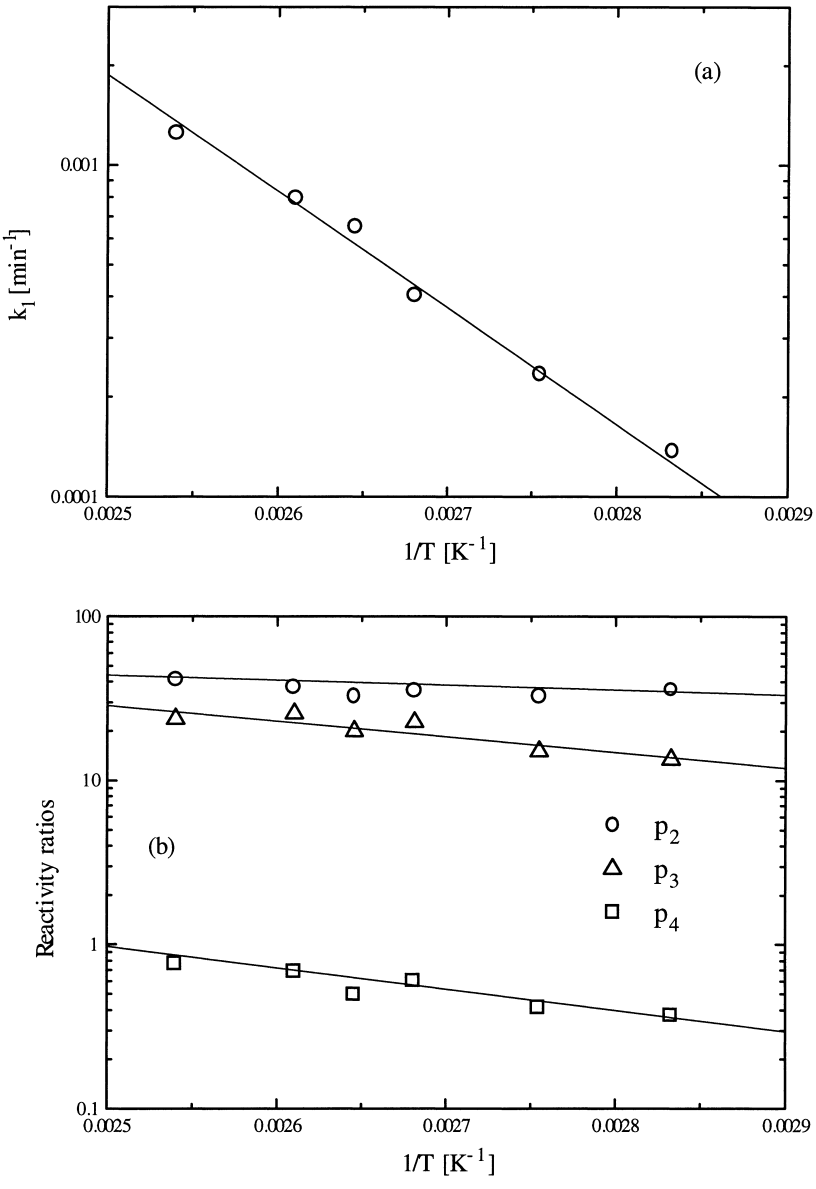

Fig. 4. Arrhenius plots for reaction rate constant k_1 (a) of lumped kinetic scheme (1) and for reactivity ratios p_j, j=2–4 (b).

above using the following relationship:

$$k_l^T = k_l^{110^\circ}\left(\frac{D_{O_2}^T}{D_{O_2}^{110^\circ}}\right), \tag{22}$$

which can be deduced from the correlations available in the literature for drops or bubbles in stirred solutions [27]. We can now compute the initial rate of oxygen uptake, as a function of temperature, by considering the reactor fed both with pure oxygen and air. The obtained values are compared with the corresponding experimental data in Fig. 2. Note that the transition from oxygen to air (i.e. the effect of diffusion limitation) at 110°C leads to a decrease of initial oxygen uptake equal to about 20%. This corresponds to the data shown in Fig. 5, which have been fitted

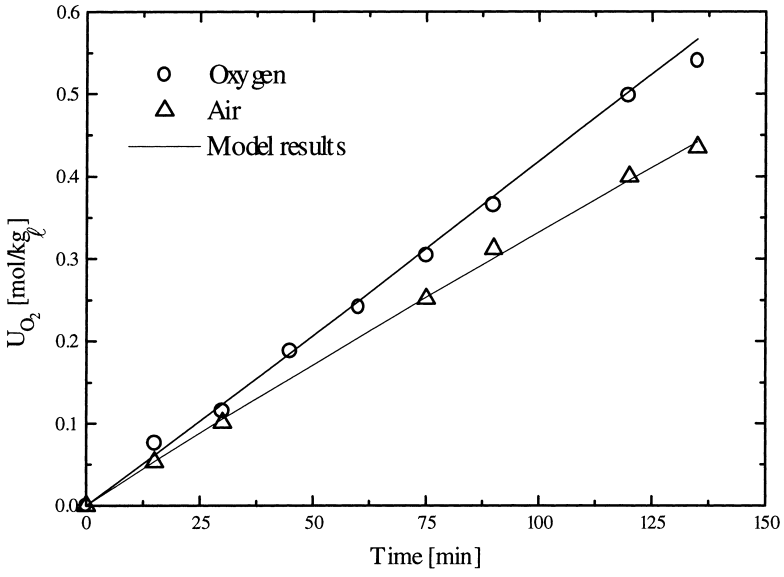

Fig. 5. Calculated versus experimental values of overall oxygen uptake, U_{O_2}, as a function of time for different oxygen partial pressures: run 10 (○) and run 11 (△) in Table 1.

against the model in order to estimate k_1. On the other hand, at T=120°C the change in the value of $R^0_{O_2}$ is much larger, i.e., about 40%, and it is well predicted by the model. A detailed comparison of measured and calculated product composition as a function of time is shown in Fig. 6 for these two runs (i.e., runs 11 and 13 in Table 1). Moreover, by decreasing the temperature values, the reactor enters the chemically controlled region and the model predictions become independent on the oxygen partial pressure. This is in agreement with the experimental data in Fig. 2, where it can be seen that the initial oxygen uptake value, measured when feeding the reactor with pure oxygen or with air are coincident.

4.3. Effect of initial concentration of p-xylene

In order to test the assumption of first-order kinetics with respect to the liquid reactant for the reactions 1–4 in the lumped kinetic scheme (1), three experimental runs (4, 7 and 15) are performed under the chemically controlled regime with different initial *p*-xylene concentration. In particular, we consider pure oxygen feed, T=100°C and the initial concentration of *p*-xylene equal to 4, 6 and 9 mol/kg$_l$, while that of *p*-tolualdehyde remains unchanged, i.e., 0.11 mol/kg$_l$. Note that no parameter has been changed in the model, whose results should then be regarded as predictions of the actual reactor behavior. The agreement with the data measured experimentally results to be satisfactory [16]. As it may be seen in Fig. 7, this model is able to predict the reactor behavior in terms of the overall rate of oxygen uptake, $R^0_{O_2}$, as a function of the initial value of *p*-xylene concentration.

4.4. Effect of catalyst concentration

A plot of the quantity U_{O_2} as a function of time for the experimental runs 12 and 18–22 in Table 1 is shown in Fig. 8. Different values of catalyst concentration are considered, while maintaining constant temperature, initial *p*-xylene and *p*-tolualdehyde concentration. The initial value of the oxygen uptake rate, $R^0_{O_2}$, was computed and plotted in Fig. 9 as a function of catalyst concentration. In the same figure the *p*-xylene conversion values reached in the corresponding experimental runs at t=60 min are also reported. It is seen that as the catalyst concentration increases both quantities first increase and then reach a plateau. Note that this behavior is consistent with that reported in the literature for *p*-xylene oxidation to *p*-toluic acid catalyzed by cobalt acetate and sodium bromine in acetic

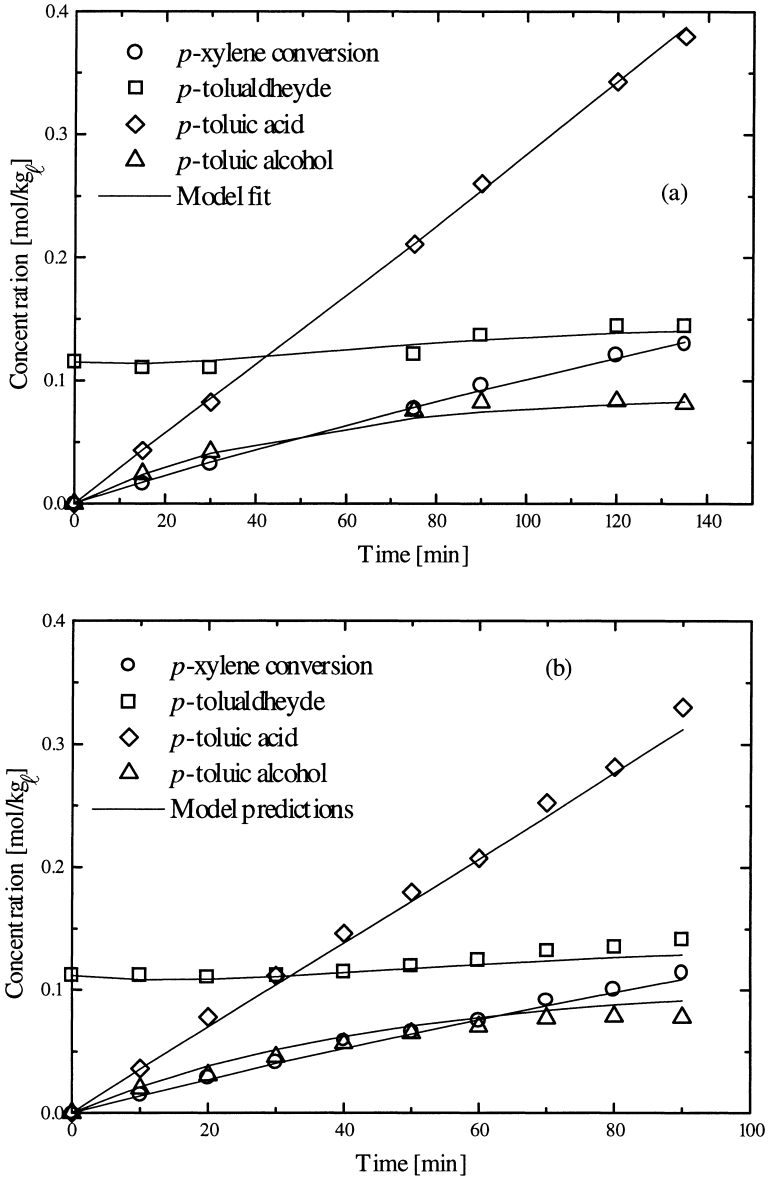

Fig. 6. Calculated versus experimental values of product concentrations as a function of time: runs 11 (a) and 13 (b) in Table 1.

acid as solvent [28]. In order to demonstrate that all experiments were conducted under the kinetic regime we have performed the experimental runs 16–18, where only the temperature values has been changed with respect to run 18. From the corresponding values of $R^0_{O_2}$ plotted as a function of temperature, a linear behavior of the Arrhenius-like is found [21], but is not reported here for sake of brevity. It may be concluded that the reactor operates in the chemically controlled regime for the specific catalyst concentration used for runs 16–18 and consequently for all catalyst concentration levels considered, at which equal or lower oxidation rates are found (cf. Fig. 9).

Due to the low *p*-xylene conversion reached during such experimental runs, only the kinetic constants of reactions 1–4 appearing in the lumped kinetic scheme

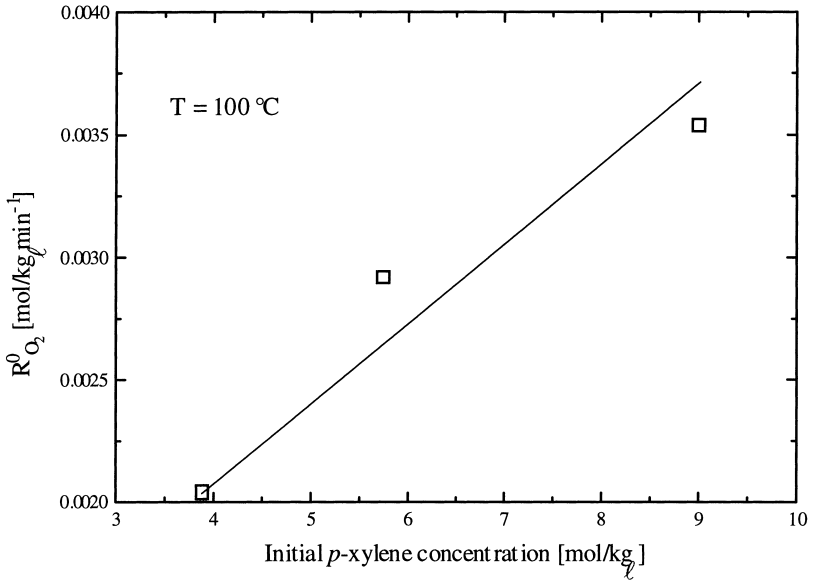

Fig. 7. Calculated versus experimental values of initial uptake rate of oxygen, $R^0_{O_2}$, as a function of initial *p*-xylene concentration: runs 4, 7 and 15 in Table 1.

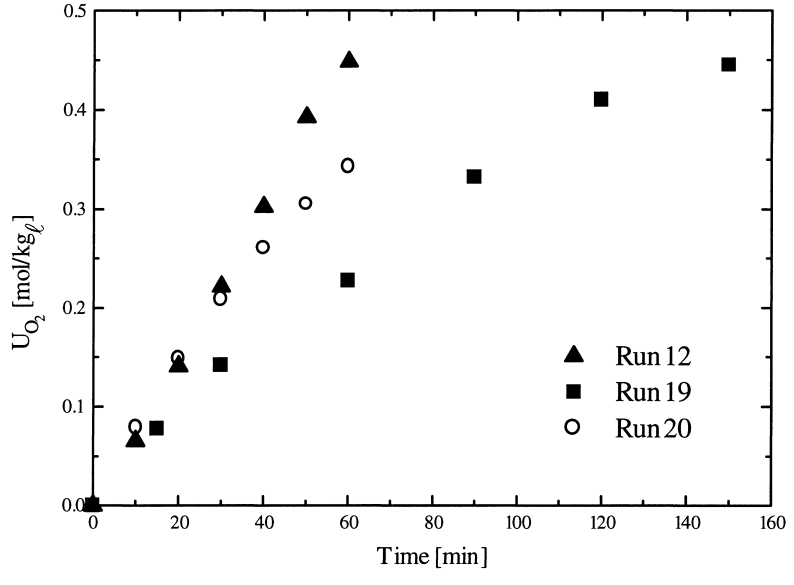

Fig. 8. Overall oxygen uptake, U_{O_2}, as a function of time for different catalyst concentrations.

(1) are then considered. These values are estimated by fitting the time evolution of the experimental product composition of run 12 and 18–22 in Table 1 through a non-linear least-square procedure using the model given by Eqs. (11) and (12). The comparison between model results and experimental data results to be generally satisfactory [21]. A representative example is shown in Fig. 10. This allows us to conclude that the lumped kinetic scheme (1) provides a level of process description detailed enough to characterize the dis-

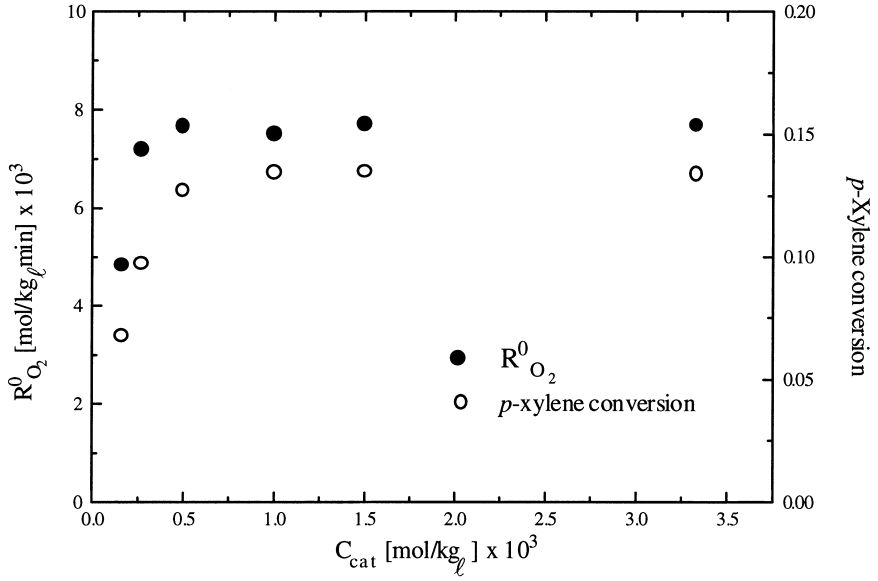

Fig. 9. Initial uptake rate of oxygen, $R^0_{O_2}$, and *p*-xylene conversion at t=60 min as a function of catalyst concentration runs 12 and 18–22 in Table 1.

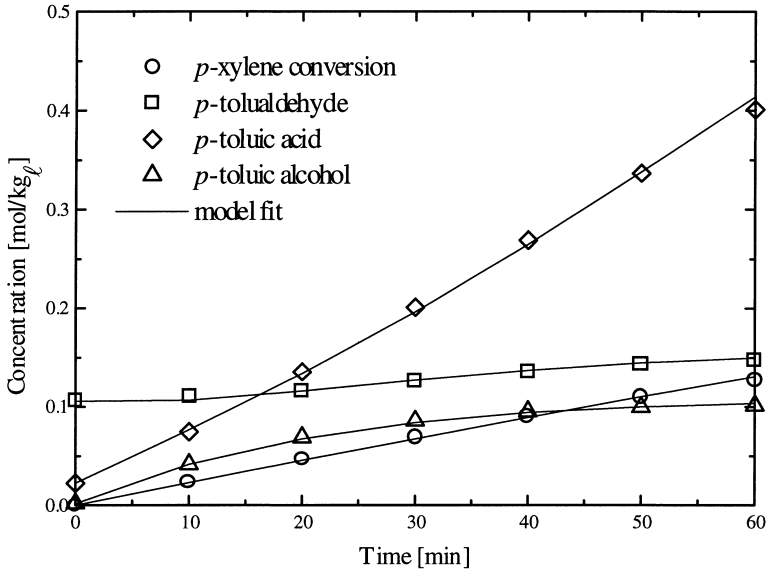

Fig. 10. Calculated versus experimental values of product concentrations and *p*-xylene conversion as a function of time: run 18 in Table 1.

tribution of the most important products even when changing catalyst concentration levels within a relatively wide range. The estimated values of k_1 and the reactivity ratios, p_j, j=2–4 at each cobalt naphthenate concentration value are summarized in Table 3, together with the average percentage error, η, arising from the fitting procedure.

From the values of the kinetic constants k_1, k_2 and k_4 which can be obtained from Table 3, it may be seen that a similar behavior of that reported in Fig. 9 for the

Table 3
Estimated values of the kinetic parameters of the lumped kinetic scheme (1) as a function of catalyst concentration

C_{cat} (mol/kg$_l$)$\times 10^4$	k_1 (min^{-1})$\times 10^4$	p_2	p_3	p_4	η (%)
1.67	4.38	71.2	59.8	1.6	6.5
2.67	7.04	69.2	71.4	1.8	4.2
5.0	11.3	45.7	35.0	1.1	1.1
10.0	12.5	41.1	23.7	0.76	2.7
15.0	11.1	41.8	41.6	1.1	2.2
33.3	11.0	44.7	45.0	1.1	4.6

case of initial oxygen rate uptake is found. This is also true for the kinetic constant k_3 only for certain range of catalyst concentration. Thus each reaction of the lumped kinetic scheme (1) may be assumed not only zeroth and first-order with respect to oxygen and the liquid reactant, respectively, as previously demonstrated, but also as dependent upon catalyst concentration through a function to be evaluated, i.e., $r_j = k_j^0 f(C_{cat}) C_i \exp(-E_j/RT)$, where C_i is the concentration of the ith component in the jth reaction. Although at this stage an empirical function, $f(C_{cat})$, can be obtained, the assumed expression of the reaction rate is in good agreement with corresponding expressions available in the literature for the consumption rate of substrate and oxygen during cobalt catalyzed oxidation of toluene in acetic acid [29], where the complex radical chain mechanism, typical of homolytic oxidations, has been accounted for. Note that the function $f(C_{cat})$ has been also assumed in the literature to contain the cobaltic and the cobaltous ion concentration, according to the presence of a monomer–dimer equilibrium of cobaltic acetate. However, since detailed radical chain mechanisms cannot be used for simulating gas–liquid reactors, as discussed in the introduction, the established dependence of the rate of each reaction of the lumped kinetic scheme (1) on catalyst concentration may have a clear practical value.

4.5. Effect of precipitation phenomena

Let us now consider the behavior of a semi-batch gas–liquid reactor where the *p*-xylene oxidation to terephthalic acid occurs together with co-precipitation of the latter one and the 4-carboxybenzaldehyde. The model equations (11)–(20) contain a large number of physicochemical parameters which unfortunately are not available in the literature for our reacting system with the exception of the kinetic constants of the lumped kinetic scheme (1) which are taken from Table 2. To overcome this difficulty and with the aim of theoretically demonstrating that the developed model properly accounts for the interaction between chemical reaction and precipitation phenomena, we consider the model parameters summarized in Table 4. Note that some of them, i.e., $C_{5,sat}$, $C_{6,sat}$, $L_{0.5}$ and $L_{0.6}$, are taken from the literature [13] even if they do not refer specifically to our system. For the parameters related to the linear growth and number nucleation rates, we select the values reported in Table 4 so that the quantities above result to be within the quite large range reported in the literature for reaction precipitation systems [10].

The time behavior of *p*-xylene, *p*-toluic alcohol, *p*-tolualdehyde, terephthalic aldehyde, *p*-toluic acid and

Table 4
Parameter values for the precipitation phenomena simulation

Parameter	Value	Reference
$C_{5,sat}$	6×10^{-6} mol kg$_l^{-1}$	[a]
$C_{6,sat}$	6×10^{-6} mol kg$_l^{-1}$	[a]
$C^0_{1,l}$	4.0 mol kg$_l^{-1}$	[16]
$C^0_{2,l}$	0.11 mol kg$_l^{-1}$	[16]
g_5	2.0	[a]
g_6	1.0	[a]
$\bar{k}_{g,5}$	8.0×10^{-7}	[a]
$\bar{k}_{g,6}$	8.0×10^{-10}	[a]
$\bar{k}_{n,5}$	6.0×10^{9}	[a]
$\bar{k}_{n,6}$	5.0×10^{4}	[a]
L_0	1.0×10^{-7} s	[a]
$L_{0,6}$	1.0×10^{-7} m$_s$	[a]
n_5	4.0	[a]
n_6	2.0	[a]
$\tilde{\rho}_{s,5}$	9.360 mol m$_s^{-3}$	[21]
$\tilde{\rho}_{s,6}$	9.350 mol m$_s^{-3}$	[21]

[a] See text for comments.

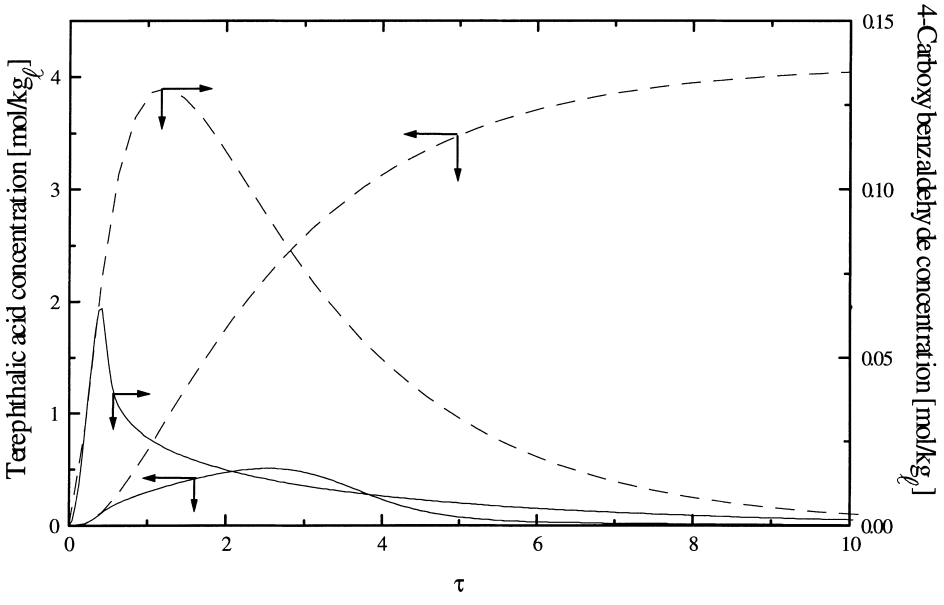

Fig. 11. Comparison between theoretical time profiles of 4-carboxybenzaldehyde and terephthalic acid concentration with (solid line) or without (dashed line) precipitation.

4-carboxybenzylalcohol, is not reported since they do not undergo precipitation phenomena and depend only upon chemical reaction on the basis of the kinetic scheme (1). As expected, all these species, except for *p*-xylene, which is continuously consumed, go through a maximum and eventually disappear from the solution. On the other hand, the effect of precipitation phenomena involving 4-carboxybenzaldehyde and terephthalic acid may be clearly seen in Fig. 11 which shows the time profiles of these two species if their precipitation is neglected, i.e. in Eqs. (12) and (13), respectively, or taken into account. In general, it may be noted that the time profile of the two species when precipitation is accounted for by the model, lie below those corresponding to the case when precipitation is not considered. In particular, 4-carboxybenzaldehyde displays the same qualitative behavior in both cases. This is because it behaves as an intermediate species and thus it is expected to first increase up to a maximum value and then decrease when consumption rate prevails. The latter one is clearly enhanced when precipitation also occurs. For the case of terephthalic acid, it is seen that its concentration increases eventually reaching a plateau if precipitation phenomena are not accounted for, since it is the only non reacting species according to the kinetic scheme (1). On the other hand, by taking precipitation into account in our model, terephthalic acid is not only formed by chemical reaction but also simultaneously precipitates, when its solution concentration exceeds the corresponding saturation value, so that the concentration profile shows a maximum in time.

Although the proposed model is able to properly simulate the time course of the crystal size distribution of 4-carboxybenzaldehyde and terephthalic acid, we do not report the corresponding results in this work due to the lack of knowledge of the appropriate model parameters related to the precipitation phenomena involved in our system. Suitable experimental studies are certainly needed in order to evaluate these parameters.

5. Concluding remarks

Some kinetic and related engineering aspects of *p*-xylene oxidation to terephthalic acid catalyzed by cobalt naphthenate are examined in this work from the experimental and theoretical point of view. The effect of various operating variables, i.e. temperature, oxygen partial pressure, initial *p*-xylene and catalyst concentration, is analyzed. A model for the description of semi-batch gas–liquid reactors for *p*-xylene

oxidation has been developed. The proposed reactor model is based on a lumping kinetic scheme of the complex radical chain mechanism of the oxidation process, where only the most important compounds detected experimentally, i.e. *p*-tolualdehyde, *p*-toluoalcohol, *p*-toluic acid, 4-carboxy benzyl alcohol, 4-carboxy benzylaldeyde, terephthalic aldehyde and terephthalic acid, are taken into account. The model accounts properly for chemical reactions, inter and intra-phase mass transfer resistances for a relatively wide range of operating conditions. This model allowed us to identify the transition from the mass transfer to the kinetic regime which may take place in the reactor, depending upon the operating conditions. The comparison between model prediction and experimental data is also presented and the agreement is quite satisfactory. The obtained results confirm the assumption that all the lumped reactions are first and zeroth order with respect to liquid reactant and oxygen, respectively. Precipitation phenomena of 4-carboxybenzaldehyde and terephthalic acid, which are both formed by chemical reaction in concentration exceeding their solubility, is analyzed theoretically by appropriate population balance equations incorporated in the semi-batch reactor model. It is shown that the time profiles of these species displays a maximum whose value depends upon the relative magnitude of the rates of reactions where these species are involved and the precipitation parameters.

It should be noted that the operating conditions as well as the catalytic system and the solvent considered in this work are different from those used at the industrial level to obtain terephthalic acid from *p*-xylene [30]. However, the approach used is quite fundamental and applicable in a straightforward manner to other conditions as well as reactor configurations, as recently shown by Markos et al. [17]. Consequently, it may provide a useful contribution towards a deeper understanding of this important process in chemical industry.

6. Nomenclature

a_v gas–liquid interfacial area per unit volume (cm^{-1})
B'_i mass based nucleation rate of the *i*th precipitating component (mol kg_l^{-1} s^{-1})
C_i concentration of the *i*th component (mol kg_l^{-1} s^{-1})
D_i diffusion coefficient of the *i*th liquid component (cm^2 s^{-1})
E_j activation energy of the *j*th reaction (cal mol^{-1})
g_i order of growth of the *i*th precipitating component
G_i linear growth rate of the *i*th precipitating component (m_s s^{-1})
G'_i mass based growth rate of the *i*th precipitating component (mol kg_l^{-1} s^{-1})
H_{O_2} Henry's constant for oxygen (cm^3 atm mol^{-1})
$\bar{k}_{g,i}$ growth rate constant of the *i*th precipitating component
$\bar{k}_{n,i}$ nucleation rate constant of the *i*th precipitating component
k_j rate constant of the *j*th reaction (min^{-1})
k_l oxygen liquid side mass transfer coefficient (cm min^{-1})
$k_{g,i}$ gas side mass transfer coefficient for the *i*th component (mol s^{-1} atm^{-1} cm^{-2})
J_i number nucleation rate constant for the *i*th precipitating component (kg_l^{-1} s^{-1})
L coordinate of particle dimension (m_s)
$L_{0,i}$ effective nucleic dimension of the *i*th precipitating component (m_s)
n_i order of nucleation of the *i*th precipitating component
N_C number of components in the system
N_i population density of particles of the *i*th precipitating component (kg_l^{-1} m_s^{-1})
N_R number of reactions in the system
p_j reactivity ratio, k_j/k_1
$p_{g,i}$ partial pressure of the *i*th component (atm)
$p_{s,i}$ vapor pressure of the *i*th component (atm)
r_j rate of the *j*th reaction (mol kg_l^{-1} min^{-1})
R_{O_2} overall oxidation rate (mol kg_l^{-1} min^{-1})
$R^0_{O_2}$ overall oxidation rate at $t=0$ (mol kg_l^{-1} min^{-1})
s distance from the gas–liquid interface (cm)
t time (s)
T temperature (K)
U_{O_2} overall oxygen uptake (mol kg_l^{-1})
x_i molar fraction of the *i*th component

Greek letters

δ liquid film thickness, D_{O_2}/k_l (cm)
ΔE_j $E_j - E_1$ (cal mol^{-1})

ϵ_l liquid holdup
η average percentage error
$\nu_{i,j}$ stoichiometric coefficient of the ith component in the jth reaction
$\tilde{\rho}_{s,i}$ crystal density of the ith precipitating component (mol m_s^{-3})
τ dimensionless time, tk_1

Subscript
cat catalyst
f liquid film
g gaseous phase
i component index
j reaction index
l liquid phase
O_2 oxygen
s solid
sat saturation conditions

Superscript
* gas–liquid interface
0 initial conditions

Acknowledgements

We gratefully acknowledge the financial support of MURST, Italy.

References

[1] R.A. Sheldon, J.K. Kochi, Metal Catalyzed Oxidation of Organic Compounds, Academic Press, New York, 1981.
[2] S. Carrà, E. Santacesaria, Catal. Rev.-Sci. Eng. 22 (1980) 75.
[3] P. Raghavendrachar, S. Ramachandran, Ind. Eng. Chem. Res. 31 (1992) 453.
[4] N.M. Emanuel, D. Gal, Modelling of Oxidation Processes, Akademiai Kiado, Budapest, 1986.
[5] M. Morbidelli, R. Paludetto, S. Carra', Chem. Eng. Sci. 41 (1986) 2299.
[6] L.K. Doraiswamy, M.M. Sharma, Heterogeneous Reactions: Analysis, Examples and Reactor Design, vol. II, Wiley, New York, 1984.
[7] R. Jacobi, M. Baerns, Erdoel Kohle Erdgas Petrochem. 36 (1983) 322.
[8] T. Mill, D.G. Hendry, in: C.H. Bamford, C.F.H. Tipper (Eds.), Comprehensive Chemical Kinetics, vol. I, Elsevier, Amsterdam, 1980, pp. 1–87.
[9] P.M. Brown, A.S. Myerson, AIChE J. 35 (1989) 1749.
[10] J. Garside, M.B. Shah, Ind. Eng. Chem. Proc. Des. Dev. 19 (1980) 509.
[11] B.l. Aslund, A.C. Rasmuson, AIChE J. 38 (1992) 328.
[12] S. Wachi, A.G. Jones, in: A. Mersmann (Ed.), Industrial Crystallization, vol. 90, GVC-VDI, Düsseldorf, 1990, pp. 229–235.
[13] S. Wachi, A.G. Jones, Chem. Eng. Sci. 46 (1991) 1027.
[14] G. Cao, A. Servida, M. Pisu, M. Morbidelli, AIChE J. 40 (1994) 1156.
[15] A. Viola, G. Cao, J. Chromatogr. Sci. 34 (1996) 27.
[16] G. Cao, M. Pisu, M. Morbidelli, Chem. Eng. Sci. 49 (1994) 5775.
[17] J. Markos, M. Pisu, M. Morbidelli, in: E. Clementi (Ed.), Methods and Techniques in Computational Chemistry, STEF, Cagliari, 1993, pp. 167–245.
[18] J. Garside, Chem. Eng. Sci. 40 (1985) 3.
[19] J.A. Dirksen, T.A. Ring, Chem. Eng. Sci. 46 (1991) 2389.
[20] A.G. Jones, J. Hostomsky, Z. Li, Chem. Eng. Sci. 47 (1992) 3817.
[21] A. Cincotti, R. Orru', G. Cao, Chem. Eng. Sci. 52 (1997) 4205.
[22] M. Hronec, J. Ilavsky, Ind. Eng. Chem. Prod. Res. Dev. 21 (1982) 455.
[23] M. Hronec, Z. Cvengrosova, J. Ilavsky, Ind. Eng. Chem. Proc. Des. Dev. 24 (1985) 787.
[24] M. Hronec, Z. Hrabe, Ind. Eng. Chem. Prod. Res. Dev. 25 (1986) 257.
[25] S.R. Bang, S.B. Chandalia, Indian Chem. Eng. 16 (1974) T92.
[26] Z. Chen, G. Li, W. Li, L. Dai, Y. Niu, J. Hu, J. Gu, X. Mao, M. Li, Int. Chem. Eng. 25 (1985) 738.
[27] P.H. Calderbank, M.B. Moo-Young, Chem. Eng. Sci. 16 (1961) 39.
[28] S.A.H. Zaidi, Appl. Catal. 27 (1986) 99.
[29] J. Hanotier, M. Hanotier-Bridoux, J. Mol. Catal. 12 (1981) 133.
[30] W. Partenheimer, Catal. Today 23 (1995) 69.